Experimental investigations on the design of a dual-media thermal energy storage with liquid metal

Franziska Müller-Trefzer[a,*], Klarissa Niedermeier[a,*], Markus Daubner[a], Thomas Wetzel[b]

[a] *Karlsruhe Institute of Technology (KIT), Institute for Thermal Energy Technology and Safety, Hermann-von-Helmholtz-Platz 1, 76344 Eggenstein-Leopoldshafen, Germany*

[b] *Karlsruhe Institute of Technology (KIT), Institute of Thermal Process Engineering, Kaiserstraße 12, 76131 Karlsruhe, Germany*

Abstract

Liquid metals are a promising heat transfer fluid with stability over a wide temperature range and high thermal conductivity. In concentrating solar energy power plants, as well as in the steel processing facilities heat is generated at high temperature level. Many fluids begin to decompose at such high temperatures and gases have poor thermal conductivity, making it difficult to effectively store and extract heat from the source. Liquid metal heat transfer fluids are able to effectively transport energy at a wide range of temperatures (150 °C–1000 °C). Existing heat transfer fluids, such as molten salts, have a working range between 290 °C and 565 °C for example. Depending on the metal selected, thermal conductivity can be 30 to 100 times higher than molten salts, but liquid metals have lower energy density. The liquid metal can be paired with a filler material having a higher energy density to develop a system with high energy transport and storage capability. The first lab-scale experiment of thermocline energy storage with liquid metal as a heat transfer fluid and a zirconium silicate filler, called VESPA [Vorversuch EnergieSPeicher Aufbau (ger.), engl. Preliminary test for energy storage setup], was carried out to prove the concept. So far, there are promising, yet only numerical investigations of thermocline energy storage with liquid metal as heat transfer fluid. The storage system under investigation was a dual-media thermocline energy storage system with liquid lead-bismuth eutectic as heat transfer fluid and zirconium silicate as filler material. The experiments were executed at temperatures from 180 °C to 380 °C, and focused on design aspects of the energy storage system. Different modes of operation of the storage system were investigated, including charging, discharging, and stand–by. Results are presented showing changes in the vertical temperature profile of the energy storage while varying mass flow, inlet temperature, and filler material.

Keywords: liquid metal, lead-bismuth eutectic, thermal energy storage, dual-media, thermocline, high temperature energy storage

1. Introduction

Advances in energy storage systems have been, and will continue to be necessary for a successful transition to larger renewable energy supplies. Energy storage systems allow energy supply and energy demand to be decoupled in terms of time. Thus, they enable the integration of energy from a fluctuating renewable energy source. In thermal energy storage systems, heat can be integrated in a direct way, such as storing heat from concentrating solar power plants, or, in an indirect way, such as using excess electricity to heat up a fluid and store it as thermal energy.

The principle of decoupling heat demand and heat supply can be used, not only for fluctuating renewable energy, but also for waste heat storage. Approximately 50% of the European energy demand is used to provide space and process heat, which corresponds to 6400 TWh per year [1]. Especially process heat generated by standard industrial processes account for a significant amount of waste heat. By using thermal energy storage systems, it is possible to use this potential energy by storing the energy first and using it later, either in form of process heat, or to generate electricity, for example, in a steam power plant.

Among the thermal energy storage systems, the sensible heat storage systems have the lowest energy density. However, they are easy to control and show the highest technical maturity compared to thermochemical and latent heat energy storage systems [2, 3]. In general, sensible heat storage systems can be classified into three different temperature levels, even though the absolute temperature of each classification differs depending on the definition. For the purpose of this investigation, the classification according to the temperature level is as follows: low (<100 °C), medium (100–500 °C) and high (>500 °C) temperature heat.

It is thermodynamically efficient to collect, store and use energy at similar temperatures. Therefore, from a thermodynamic point of view, maintaing high temperature

*Corresponding authors

Email addresses: franziska.mueller-trefzer@kit.edu (Franziska Müller-Trefzer), klarissa.niedermeier@kit.edu (Klarissa Niedermeier)

levels of the storage media provides the greatest heat recovery potential [1, 4]. The heat at a high temperature level can be either used as process heat or can be transformed to electricity. For the latter, higher temperature levels lead to higher conversion efficiencies.

Storing high temperature media is challenging, due to limitations on suitable heat transfer fluids (HTF) and materials for the heat storage including housing and instrumentation. However, liquid metals are promising options as HTFs since they have high heat conductivity, which leads to a high heat absorption efficiency, as has been shown for several applications as for concentrating solar and nuclear power plants [5, 6, 7, 8, 9, 10, 11]. Liquid metals are also proposed for thermal energy storage [12, 13, 14]. Furthermore, they are stable in a wide temperature range, so that a thermal energy storage system using liquid metal as HTF can be operated not only at high temperature but also in a wide range down to medium temperature levels. In this study, a lead-bismuth eutectic (LBE) was used, which has a melting point of 124.8 °C and is stable above 1000 °C [15]. LBE is corrosive, particularly at high temperatures [16, 17], limiting the maximum temperature it can be used in various housing materials. Ongoing research promises new corrosion-resistant structural materials so that LBE can be used as HTF at temperatures above about 550°C [18, 19].

Stratified (thermocline, single-tank) storage systems are attractive thermal energy storage systems in terms of economic aspects, which was shown in literature for molten salt as heat transfer [20, 21]. However, using a liquid metal HTF with a high heat transfer coefficient, is contradictory to maintaining a stable thermocline. Thus, a dual-media thermocline heat storage solution is proposed. The thermocline energy storage is filled with a solid granular filler material with high heat capacity and low conductivity to stabilize the stratification in the thermal heat storage. Numerical investigations have shown that a dual-media thermocline heat storage with LBE as liquid metal is a promising concept [3]. A dual-media thermocline energy storage with LBE is planned to be built at the Karlsruhe Liquid Metal Laboratory (KALLA). Before building the test facility DUO-LIM (DUal-Media thermocline energy storage with LIquid Metal), a lab-scale prototype, named VESPA (*Vorversuch EnergieSPeicher Aufbau* (ger.), engl. preliminary test for energy storage setup) was installed and is the focus of this investigation. To the best of the authors' knowledge, VESPA is the first-of-its-kind dual-media thermocline energy storage solution implementing LBE as heat transfer fluid, and a ceramic high heat capacity filler. Primary results are presented with focus on the design of larger thermocline energy storage system based on this concept.

2. The VESPA experiment

The VESPA experiment is a preliminary test for the design and scale-up of the dual-media thermocline heat storage (DUO-LIM) with a storage volume of around 0.5 m^3, and a potential energy storage capacity of around 100 kWh. The heat storage volume of the VESPA experiment is about 0.005 m^3, which corresponds to about 1 kWh of energy storage – 100 times smaller than the DUO-LIM storage volume.

2.1. Working principle of the test facility

The VESPA test facility consists of three tanks: an energy storage, a cold reservoir, and a hot reservoir. It is shown schematically in Fig. 1 and as a picture in Fig. 2.

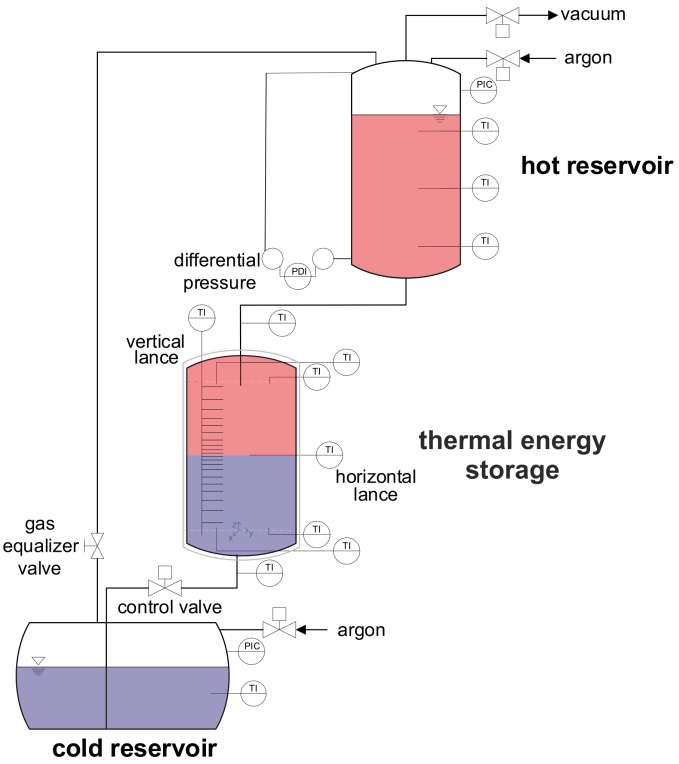

Figure 1: Schematic of the test setup of the VESPA test facility

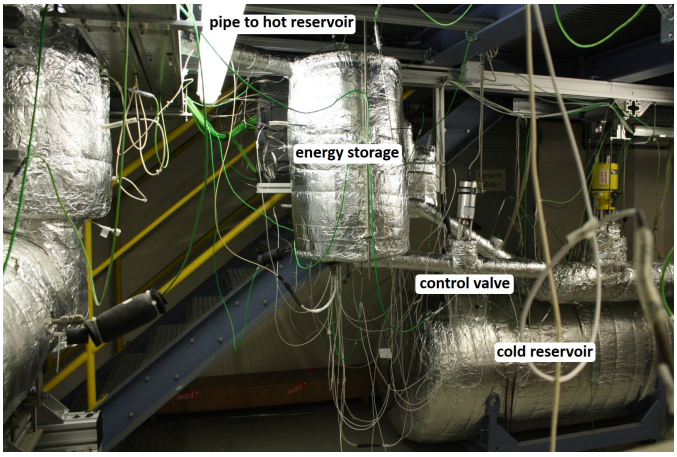

Figure 2: Photo of the setup of the VESPA test facility, photo: Katja Dieterle/KIT

The three tanks of the test facility are at different heights, as shown in Fig. 1. The lowest point of the experi-

ment is the cold reservoir so that in case of an emergency, the liquid metal can be drained into this tank. The hot tank is the highest point and the energy storage is in between the two reservoirs. LBE flows through the main pipe connecting the cold tank, energy storage, and hot tank. This pipe contains a control valve to regulate the LBE mass flow. In addition, another pipe with a gas equalizer valve connects the two gas compartments. Since the VESPA facility does not have a pump, the mass flow for charging and discharging is realized through the interaction of gas pressure gradients between the two reservoirs, and the geodetic pressure.

Before each (dis)charging cycle, a homogeneous temperature was adjusted in the energy storage and the relevant reservoir tank. Afterwards, the heaters of the energy storage were turned off and the control valve was opened to adjust the mass flow rate. The mass flow during charging occurred mainly due to gravity, and the gas equalization valve was open at the same time. In order to discharge, the pressure of the gas compartment of the cold tank is increased so that the pressure difference between the two gas compartments was high enough to realize the mass flow against gravity.

All liquid-metal containing components were insulated with rock wool. To prevent the HTF from solidifying, heaters were installed on all tanks as well on the piping and on the valves. The LBE temperature was always kept above 180°C.

2.2. Energy storage tank

The energy storage reservoir tank in Fig. 3 is made of stainless steel (1.4571) and consists of a cylindrical body which is closed with a flange at the bottom and the top. On the inside of the energy storage, next to the flanges, there are two sintered metal filters (shown in blue in Fig. 3), which enclose the storage volume and ensure that no particles of the filler material, which could be created by abrasion can pass through the fluid into the reservoir tanks. The packed bed in the energy storage reservoir tank has a bed diameter of 130 mm and a height of 374 mm. The filler material consists of a zirconium silicate grinding media (Rimax, ZirPro, Saint Gobain) with a diameter range of 2.5 mm–2.8 mm. The density of the zirconium silicate spheres ρ_{Rimax} was determined with a pycnometer to be $4204 \pm 23\,\mathrm{kg/m^3}$ at room temperature. Due to the low thermal expansion of zirconium silicate, the density was assumed to be constant over the entire temperature range investigated in this paper. Since the mass of the spheres in the packed bed $m_{\mathrm{packed\ bed}}$ in the energy storage (ES) was determined, the porosity Ψ can be calculated with the volume enclosed by the filter V_{ES} without the volume of the thermolances (see section 2.4) $V_{\mathrm{instrumentation}}$ by Eq. 1.

$$\Psi = 1 - \frac{V_{\mathrm{ES}} - V_{\mathrm{instrumentation}}}{\frac{m_{\mathrm{packed\ bed}}}{\rho_{\mathrm{Rimax}}}} \tag{1}$$

This results in a porosity of about 0.36. The determination of the porosity of the packed bed in the energy storage was repeated 3 times, and the porosity was always between 0.36 and 0.37. The thermal conductivity, as well as the heat capacity of the Rimax beads was determined by the producer Saint Gobain [22] and is shown in Tab. 1. The filler material selection is described in more detail in section 2.3.

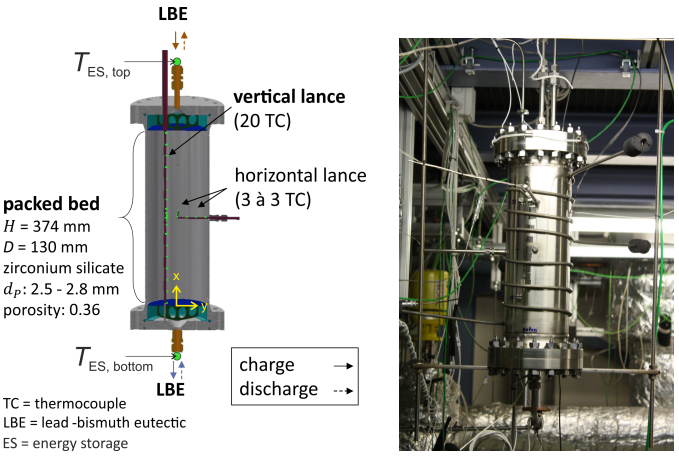

Figure 3: Left: CAD model of the energy storage compartment; right: picture of the energy storage container before insulation (photo: Katja Dieterle/KIT)

The calculations used to determine the material properties of the LBE are found in Eq. 2 to 5.

The density of LBE ρ_{LBE} in $\mathrm{kg\ m^{-3}}$ was calculated by using Eq. 2 [15].

$$\rho_{\mathrm{LBE}} = 10981.7 - 1.1369 \cdot T \tag{2}$$

The heat capacity of the LBE $c_{p,\mathrm{LBE}}$ in $\mathrm{J\ kg^{-1}K^{-1}}$ was caluclated by using Eq. 3 [15].

$$c_p = 164.8 - 3.94 \cdot 10^{-2} \cdot T + 1.25 \cdot 10^{-5} \cdot T^2 - 4.56 \cdot 10^{5} \cdot T^{-2} \tag{3}$$

The thermal conductivity of the LBE λ_{LBE} in $\mathrm{W\,m^{-1}K^{-1}}$ was determined using Eq. 4 [15].

$$\lambda_{\mathrm{LBE}} = 3.284 + 1.617 \cdot e^{-2} \cdot T - 2.305 \cdot e^{-6} \cdot T^2 \tag{4}$$

The dynamic viscosity of the LBE μ_{LBE} in Pa s was calculated by using Eq. 5 [15].

$$\mu_{\mathrm{LBE}} = 4.94 \cdot 10^{-4} \cdot e^{\frac{754.1}{T}} \tag{5}$$

In all four cases, T refers to the temperature in K. The presented material properties were calculated for a temperature of 250°C and are listed in Tab. 1.

2.3. Filler material selection

In the dual media thermocline energy storage experiment, the filler material was selected to be compatible with the heat transfer fluid within the operating range of the system. A low heat conductivity was desired in order to diminish the growth of the thermocline and a high energy storage density was also desired to achieve a compact and effective thermal storage system. This means a material

Table 1: Parameters of VESPA energy storage as well as material properties

	parameter	value	units
packed bed	diameter	130	mm
	height	374	mm
	porosity	0.36	-
filler [a]	material	zirconium silicate	-
	diameter	2.5–2.8	mm
	$\rho_{\mathrm{T=20°C}}$	4204	kg m^{-3}
	$c_{p,\mathrm{T=250°C}}$	1.01	J g^{-1}K^{-1}
	$c_{p,\mathrm{T=500°C}}$	1.28	J g^{-1}K^{-1}
	$\lambda_{\mathrm{T=250°C}}$	7.7	W m^{-1}K^{-1}
	$\lambda_{\mathrm{T=500°C}}$	7.2	W m^{-1}K^{-1}
HTF [b]	material	LBE	-
	T_{melt}	123.8	°C
	$\rho_{\mathrm{T=250°C}}$	10 387	kg m^{-3}
	$c_{p,\mathrm{T=250°C}}$	0.15	J g^{-1}K^{-1}
	$\lambda_{\mathrm{T=250°C}}$	11.11	W m^{-1}K^{-1}
	$\mu_{\mathrm{T=250°C}}$	$2.09 \cdot 10^{-3}$	Pa s

[a] properties filler from Saint Gobain [22]
[b] properties HTF from Ref. [3]

with a high heat capacity c_p as well as a high density ρ would be needed. Due to the working principles of the system, a filler material with thermal shock resistance, as well as a resistance to thermal cycling was necessary. A low-cost material would, of course, also be beneficial in view of later industrial application.

Based on the previously mentioned criteria, three main categories of materials (glasses, ceramics and natural stones) were investigated in more detail. The potential filler materials were stored in LBE at a temperature of 500 °C for one week, and then four weeks under reducing atmosphere. The materials were then evaluated by comparing scanning electron microscope (SEM) images and energy dispersive X-ray spectroscopy (EDX) spectra. The analysis showed that zirconium silicate was the most promising filler material for this application, since no optical changes of the surface could be identified with the SEM and the samples also had no cracks, which would indicate insufficient thermal shock resistance. The analysis with EDX also did not show any change in composition of the material that would indicate a dissolution of certain ceramic components.

2.4. Measurement of temperatures and pressure difference

A precise temperature measurement is necessary to evaluate the performance of the thermal energy storage system. Therefore, 30 type-K thermocouples were integrated in the energy storage by a vertical lance (20 thermocouples) and by two horizontal lances which were arranged in the shape of a T (10 thermocouples). The thermolances are small tubes with tiny holes of diameter 0.5 mm for each of the 30 thermocouples. They pass through a hole and are guided by a pin (vertical lance) or a hole (horizontal lance) on the opposite site. There was always a small gap between the pipe end and the structural tank material to prevent thermal stress and bending of the lances, but it was less than 1 mm. The thermocouples were glued with a thermally stable ceramic adhesive (Thermeez Hi Seal 7030, Polytec PT) so that the tip of the thermocouple protruded circa 1 mm from the surface of the thermolance. Due to the defined position of the thermocouple lances, the position of every temperature measuring point was well defined. Furthermore, the temperature of LBE at the inlet and outlet of the heat storage was measured by a type-K thermocouple (diameter 3 mm), referred as $T_{\mathrm{fluid,top}}$ or $T_{\mathrm{fluid,bottom}}$ in Fig. 3. The thermocouples at the inlet and outlet pipe of the energy storage, as well as the thermcouples on the inside of the energy storage container were calibrated by a dry well calibrator in the range of 200 °C to 400 °C.

The mass flow was determined by a differential pressure measurement in the hot tank. Due to the change of the level of fluid in the hot tank during charging or discharging, the differential pressure changes, from which the mass flow ($\dot{m}$)(change in mass in the hot reservoir) Δm per time Δt can then be determined by the following equation:

$$\dot{m} = \frac{\Delta m}{\Delta t} = \frac{\pi \cdot \mathrm{r}^2}{g} \cdot \frac{\Delta p}{\Delta t}, \tag{6}$$

where $\pi \cdot \mathrm{r}^2$ is the cross-sectional area of the hot tank and g stands for gravitational constant. The change in the pressure gradient Δp was measured by a coplanar pressure transmitter (Rosemount$^{\mathrm{TM}}$3051SCD Coplanar$^{\mathrm{TM}}$ Pressure Transmitter) with two pressure measuring flanges (diaphragm seal system). Both pressure measuring flanges are at the same height. The pipe of one flange leads to the head of the hot reservoir in the gas phase, while the pipe of the other leads to the lowest point in the hot reservoir in the LBE.
The fluid velocity in the fixed bed in the energy storage reservoir can than be calculated by Eq. 7:

$$v_\Psi = \frac{\dot{m}}{\rho_{\mathrm{LBE}}(T_{\mathrm{LBE}}) \cdot \pi \cdot \frac{D_{\mathrm{ES}}^2}{4} \cdot \Psi} \tag{7}$$

with the inlet mass flow $\dot{m}$, the density of LBE ρ_{LBE} at the temperature of the fluid T_{LBE}, and the cross-sectional area of the energy storage (ES) $\pi \cdot \frac{D_{\mathrm{ES}}^2}{4} \cdot \Psi$.

3. Experimental Parameters

In this section, the operating parameters will be discussed first, followed by the evaluation parameters.

3.1. Operating parameters

Each experiment consists of two periods; charging or discharging, and a subsequent standby phase, as shown in Fig. 4. Thus, the influence of (dis)charging on the standby phase can be determined. Before (dis)charging, the temperature in the energy storage was set and maintained

at a homogeneous temperature with the help of the four surrounding heaters. This means that the temperatures in the vertical lance never differed more than 1.2 K.

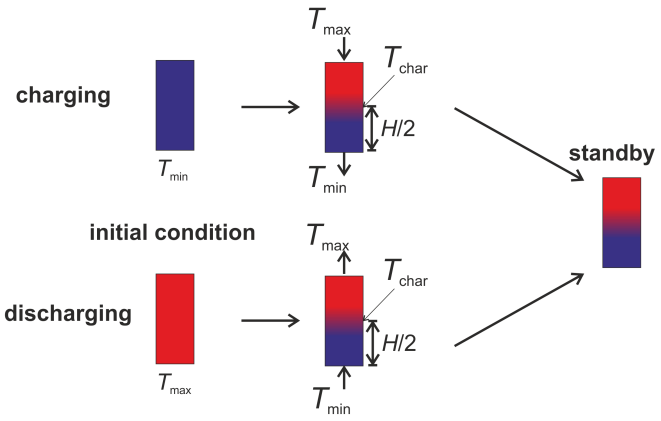

Figure 4: Schematic of the operation of the VESPA test facility. Here, (dis)charging experiments are carried out until the characteristic temperature has reached at half that of the energy storage, followed by a standby experiment.

The influence of the flow velocity through the packed bed was investigated for (dis)charging as well as for each following standby phase. The applied temperature gradient was always 200 K at the beginning of (dis)charging phase with a minimal temperature of 180 °C. The temperature in the energy storage before charging, the corresponding inlet temperature, and the applied pore velocity in the energy storage ($v_{\Psi,\mathrm{set}}$) are shown in Tab. 2. All experiments shown in the table are performed analogously for discharging. This means the temperature difference was kept constant for discharging, but the energy storage had a temperature of 380 °C at the beginning of the experiment, and the fluid entered with a temperature of 180 °C . The thermocouples are not arranged equidistantly along the vertical thermolance axis, but the distance between the thermocouples decreases towards the center. The position of the thermocline is defined by a characteristic temperature T_{char}. The characteristic temperature is the mean of the temperature at the top ($T_{\mathrm{top,ES}}$) and the bottom ($T_{\mathrm{bottom,ES}}$) of the vertical lance in the energy storage and is described by the following equation (Eq. 8):

$$T_{\mathrm{char}} = 0.5 \cdot T_{\mathrm{top,ES}} + 0.5 \cdot T_{\mathrm{bottom,ES}} \tag{8}$$

Therefore, if the thermocline is in the center of the tank, this corresponds to a (dis)charging of half of the tank, as it is shown in Fig. 4.

3.2. Evaluation parameters

In order to be able to compare the temperature profiles in the energy storage at various operating conditions, such as at different temperature levels or at different mass flow rates, non-dimensional numbers are defined. Eq. 9 is proposed to describe the temperature in the energy storage T as non-dimensional temperature Θ.

Table 2: Parameters of experiments

$v_{\Psi,\mathrm{set}}$ [a] mm s^{-1}	$T_{ES(t=0)}$ °C	T_{in} °C	ΔT K	(dis)charging state –
0.43	180 (380)	380 (180)	200	half
0.88	180 (380)	380 (180)	200	half
1.17	180 (380)	380 (180)	200	half
1.74	180 (380)	380 (180)	200	half
2.33	180 (380)	380 (180)	200	half

[a] v_Ψ= pore velocity in the energy storage according to Eq. 7.

$$\Theta = \frac{T - T_{\mathrm{min}}}{T_{\mathrm{max}} - T_{\mathrm{min}}} \tag{9}$$

For a charging process, the temperature in the energy storage is defined by T_{min} and T_{max} is the inlet temperature, measured in the fluid entering the energy storage. For a discharging process, T_{min} is the LBE inlet temperature and T_{max} is the temperature in the energy storage at the beginning of the experiment.
As a result of varying the mass flow, the time of charging and discharging varies, as well as the change of energy in the energy storage per time. Therefore, in order to compare the experiments, a non-dimensional time τ is used, by dividing the absolute time t by the complete experiment time t_{total} (charging, discharging or standby) as defined in Eq. 10.

$$\tau = \frac{t}{t_{\mathrm{total}}} \tag{10}$$

4. Results

In the following, the results of the experiments are presented.

4.1. Stability of inlet parameters

The mass flow is determined using Eq. 6 mentioned above. The determination of the change in pressure difference is challenging due to the small mass flows and consequently small differential pressure changes. The uncertainty of the differential pressure transmitter is specified as 0.075% of the measuring span. This leads to a total error of 1.86 mbar. If the change in differential pressure was discretized as a function of time $\frac{\delta p}{\delta t}$, a noisy signal is obtained. On the other hand, when considering the absolute differential pressure as a function of time, a mainly

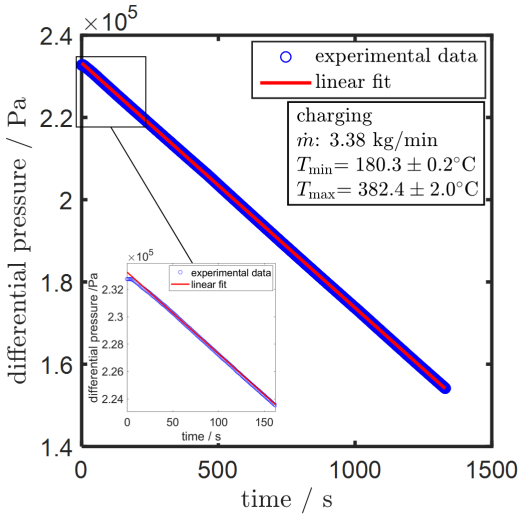

Figure 5: Experimental data of the differential pressure (blue), measured in the hot tank, depending on time for a mass flow of 3.38 kg/min and a linear fit of the experimental data (magenta).

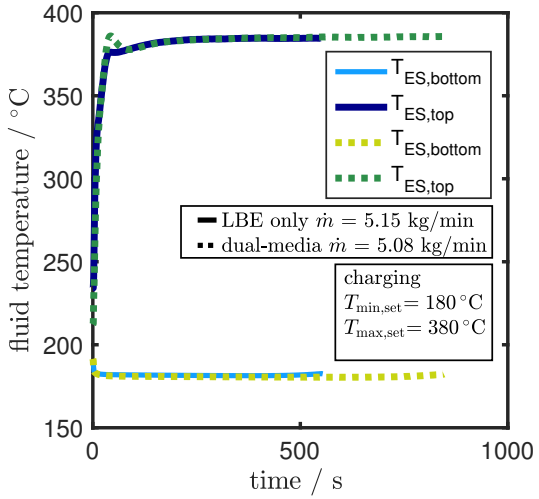

Figure 6: Characteristic temperature profile for the inlet and outlet temperature $T_{\mathrm{ES,top}}$ and $T_{\mathrm{ES,bottom}}$ of the energy storage for a charging process with LBE only (solid line) and with zirconium silicate as filler material (dashed line).

linear change in differential pressure was observed, which indicates a stable mass flow, as can be seen in Fig. 5.

Therefore, the change in differential pressure is fitted as a function of time with a linear function and then, to specify a standard uncertainty, the standard deviation of the measurements from the fit function are determined. The slope corresponds to the pressure change per time. At the beginning of the (dis)charging process, the differential pressure change does not show a linear characteristic, since the control valve was opened first and some time was needed to set the required mass flow, as is shown in Fig. 5. In particular, the time taken to set the desired mass flow at the start of the experiment can have an influence on the subsequent temperature profiles. The pressure change per time can be described very well with the help of a linear regression. Here, a minimum of 86% of the measured values are within 1% deviation. A non-linear pressure change also occurs when closing the valve. Both the opening and closing of the valve are included in each experiment and took between 3 s and 19 s at maximum until the target value of the preset opening of the valve (in percent) was reached. This time was depended on the target value. Since the experiments are non-steady-state experiments and the opening and closing of the valves is necessary in all tests, they were taken into account when determining the linear regression and the standard deviation of the measured values from the linear regression.

Another important parameter when comparing different measurements is the inlet temperature. When using the dimensionless temperature, the temperature stability of the inlet temperature is particularly relevant as it is used as reference. Two exemplary temperature profiles of the inlet and the outlet temperatures of the energy storage are shown in Fig. 6 over time.

Here the fluid temperatures at a comparable mass flow (about 5.1 kg/min) are considered once for the case that only LBE is in the energy storage (solid line) and once that zirconium silicate and LBE (dual-media) are in the storage.

In case of the dual-media setup, it is noticeable that the inlet temperature (dark green) shows an overshoot before the temperature becomes constant. This is related to the heating of the hot tank. All pipes and tanks are equipped with trace heaters, which are each controlled by using a thermocouple applied to the surface. Since the heaters are not applied perfectly homogeneously on the surface, and the power of the heater depends on the temperature measured at one position of the corresponding thermocouple, it may happen that some points along the wall may not be completely homogenous in temperature. In addition, discharging and charging are transient processes. Therefore, a target temperature (T_{target}) was determined and the time (t_{const}) after the inlet temperature reached $T_{\mathrm{target}} \pm 5\,K$ for the first time of the experiment. The target temperature was defined as the average of the last 100 measured values ($\approx$ 104 s). The inlet temperature averaged over the entire experimental time was referred to as T_{in}. The calculated characteristic temperatures and standard deviations for the measurements considered in Fig. 6 are given in Tab. 3.

Table 3: Determination of the characteristic inlet temperature based on experimental data presented in Fig. 6

experiment	t_{const} min	$t_{\mathrm{const}}/t_{\mathrm{total}}$ %	T_{target} °C	T_{in} °C
LBE only	7.5	80.8	384.4 ± 0.2	381.8± 2.4
dual-media	13.5	95.9	385.4 ± 0.1	383.1± 2.3

In the test without filler, the heating was not ideal

and, due to the geometry of the hot tank, a temperature stratification occurred. In the experiments with filler, an additional heater was installed so that the temperature homogeneity in the hot tank is improved, as can be seen by the lower run-in time compared to the total experimental time, which decreased from 19.2 to 4.1%.

However, since the actual inlet temperature is used for the calculation of the dimensionless temperature, this influence can be neglected in the dimensionless case. The outlet temperatures of the two experiments were approximately constant until the end of the experiment, which implies that the thermocline was still completely in the energy storage.

4.2. Comparison of charging and discharging

Fig. 7 shows results from a charging (grey symbols) and discharging (blue symbols) process, which were operated with the same mass flow. The temperature difference between the LBE at the inlet of the energy storage and the temperature in the energy storage at the beginning of the experiment was about 200 K for both charging and discharging. The dimensionless temperature profiles along the vertical axis for different time steps are presented for these parameters. As described before the (dis)charging process was realized until T_{char} was reached at half of the height of the energy storage. The temperatures along the vertical axis are shown at the beginning of the process, after 25%, 50%, 75% of the process time, as well as at the end. The absolute process time for the total charging and discharging process was about 22.5 min in each case.

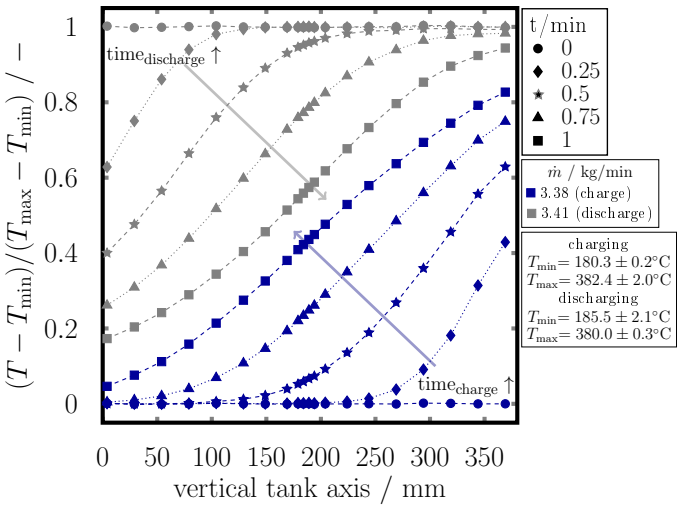

Figure 7: Temperature along the vertical axis of the energy storage filled with zirconium silicate spheres. Charging (blue markers) and discharging (grey markers) processes are shown with a mass flow of 3.4 kg/min for a temperature difference of about 200 K.

When the center of the energy storage reached the required temperature, the thermocouple at the top of the vertical lance had not yet reached the temperature of the incoming LBE fluid stream for a charging process. It can be seen from Fig. 7 that only about 80% of the maximum relative temperature was reached at the top of the vertical lance in the experiment. This temperature difference can have various reasons. On the one hand, it may be due to the good thermal conductivity of the HTF. If the heat were to be transferred to the region with lower temperature, and thus to the lower part of the energy storage as it enters, this would result in a lower temperature at the very top of the energy storage. On the other hand, the mass of the flanges of the energy storage, and consequently their heat capacity, is huge compared to the incoming fluid as well as the entire storage volume. Table 4 gives an overview of the heat storage capacities of different parts of the energy storage calculated by their masses and material heat capacities. It should be kept in mind that the heat storage capacities presented here are specific for the lab-scale preliminary experiment VESPA. The unfavorable heat storage capacity ratio of the main energy storage (fixed bed + LBE) to the structural material of the tank is due to the small size of the energy storage. For larger tanks, the heat storage capacity of the tank plays a minor role or no role at all.

Table 4: Heat storage capacity

part of energy storage	specification	heat storage capacity[1] / kWh
ideal storage	LBE only	0.43
volume [2]	LBE + filler	0.91
structural	one flange	0.22
material [3]	entire tank	0.56

[1] calculated, ideal charging assumed
[2] volume in between the two sinter filters
[3] made of stainless steel

It can be concluded that zirconium silicate as filler approximately doubles the heat storage capacity. For charging up to the center of the energy storage, one flange must be heated in addition to a part of the packed bed. Almost one third of the energy from the LBE is needed just for heating up the flange. Thus, the entering fluid needs to heat up not only the packed bed in the energy storage, but also the flange at the top of the energy storage. As a result, after passing the flange, the fluid probably already transferred a part of its energy to the flange so that the fluid entered the packed bed at a lower temperature, as measured at the inlet pipe of the energy storage. In addition, due to the relatively small cross-sectional area of the incoming LBE flow compared with the total flange area, heating of the flange to the inlet temperature of the LBE takes some time. At least at the beginning, the fluid will therefore also transfer heat to the flange, and consequently the temperature of the fluid entering the packed bed of the energy storage is lower than the inlet temperature.

Furthermore, at the beginning of charging, the hot incoming fluid mixes with the cold fluid (initial condition)

located in the energy storage between the flange and the sinter filter. It is the same vice versa for the inlet flow during the discharging process. The area between the fluid inlet and the sinter filter is hereafter referred to as the mixing area. This area has been designed with flow disturbers in such a way that the fluid enters the packed bed with as homogeneous a velocity as possible over the entire cross-sectional area of the sinter filter. The several flow distributors lead to an intensive exchange of the stagnant and the incoming fluid, which consequently also leads to a mixing of the temperature. Fig. 8 shows different temperatures measured during the charging process over time. The inlet temperature, measured at the inlet pipe (green triangles), reached an almost constant value. The temperature measured directly at the filter (blue squares) and the temperature measured at the highest point of the vertical thermocouple lance (red dots) show an exponential curve. The temperature of the sinter filter and the top thermocouple of the thermocouple lance did not deviate by more than 3.4 K. This deviation may indicate inhomogeneous mixing in the mixing area, but it may also be due to the uncertainty of the temperature measurement of the reference junction, which was different for the thermocouples of the vertical lance than for the thermocouples in the filter.

In order to describe the influence of the fluid temperature entering the packed bed, further investigations are required, either numerically or by inserting further thermocouples.

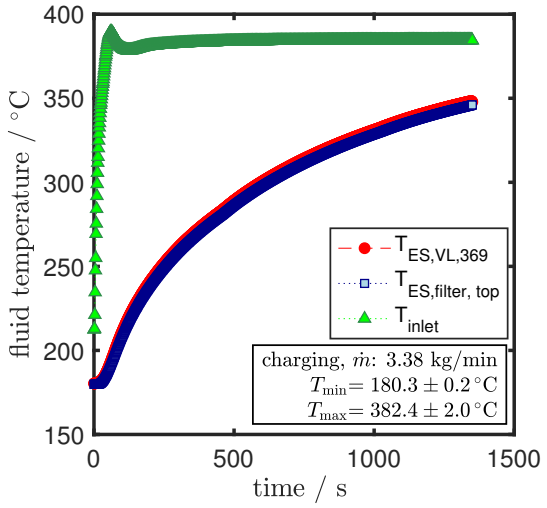

Figure 8: The inlet temperature (green triangles), the temperature measured at the filter (blue squares) and the temperature at the highest position of the vertical thermocouple lance (369 mm from the sinter filter of the bottom (red dots) are shown over time during a charging experiment.

4.3. Influence of the inlet temperature on the stratification

As can be seen from Fig. 8, there was no temperature step of the fluid entering the packed bed, but rather an exponential curve of the temperature directly at the inlet of the fluid into the packed bed. The influence of the inlet temperature on the temperature profile during the charging process is investigated numerically.

The numerical model was developed by Niedermeier et al. and is described in detail in Ref. [23]. The model is developed for a large energy storage and assumes a uniform velocity over the fixed bed and that the boundary effects are negligible due to the size of the energy storage. The dual-media energy storage presented here is a preliminary test in which boundary effects and heat losses have a major influence due to its unfavorable volume to surface ratio. Nevertheless, the goal is to consider important design aspects, so this is why numerical investigations are referred to for this evaluation.

Two different temperature profiles of the entering LBE into the packed bed are investigated, which are shown in Fig. 9: first, a temperature profile with an ideal temperature being T_{max} during the entire charging process (dashed line) and second, the temperature profile as also measured in the VESPA experiment at the uppermost thermocouple of the vertical lance (solid line). Fig. 10 shows the resulting temperature profiles in the energy storage at the beginning of charging, after 25%, 50 %, 75% and after the entire charging time (thermocline is in the center of the energy storage). The marks in Fig. 10 represent the discrete measured values, the solid lines are the temperature profiles of the temperature entering the packed bed, as in the VESPA experiment, and the dashed line is the temperature profile to be expected when the fluid enters the packed bed with T_{max} during the entire charging process.

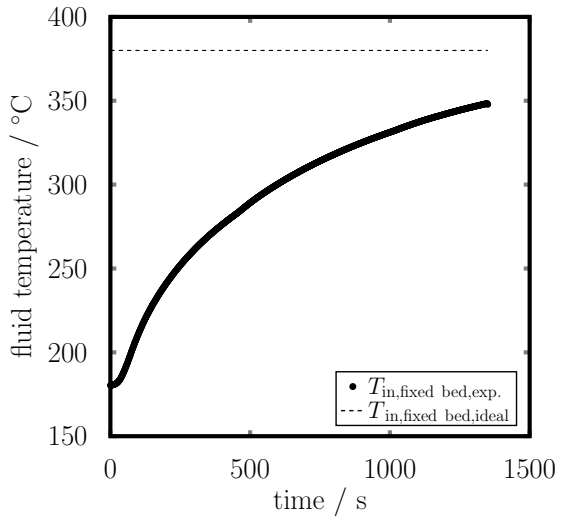

Figure 9: Inlet temperature of the LBE in the fixed bed in the energy storage during charging. The experimentally determined temperature (dots) is the same as $T_{\mathrm{ES,VL,369}}$ presented in Fig. 8. The dashed line describes the ideal temperature entering the fixed bed, which is at T_{max} during the entire charging period.

The numerical simulation results differ from the experimental temperature profiles partially due to the assumption of ideal conditions when executing the numerical simulation. The temperature profiles in the energy storage during charging with a step-change inlet temperature into the

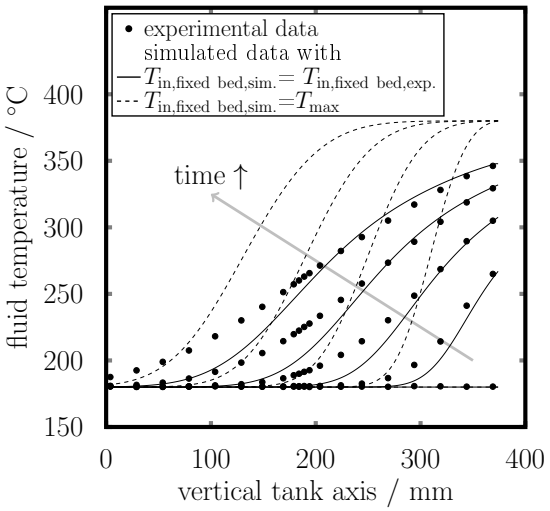

Figure 10: Temperature profiles during charging at the beginning, after 25%, 50%, 75% and at the end of the charging process. Experimental data (dots) and simulated data (lines) are shown. The simulated temperature profiles result either from the inlet temperature determined experimentally (solid line) or from the ideal inlet temperature (dashed line). The inlet temperatures are shown in Fig 9.

packed bed are clearly steeper than the temperature profiles with a slowly increasing inlet temperature. In the case of the temperature profile with the slowly rising inlet temperature, after the defined charging time (the temperature in the middle of the storage tank is the average value of the current minimum and maximum temperature in the energy storage), no area with hot and cold zones can be identified in the energy storage tank. Instead, a continuous temperature stratification extends over the entire storage tank. In the case of a step-change inlet temperature, two temperature areas with a thermocline layer in between can be observed at the end of the charging process. The numerical simulations show that an inlet temperature of $T_{\max}$ during the entire charging process over the entire cross-section of the energy storage has a beneficial effect on the temperature stratification and separation of the hot and cold area in the energy storage. Even if some assumptions are certainly idealized in this simulation, care should be taken in the design of an energy storage with liquid metal to make the mixing zone as effective as possible. This means that the entry velocity into the packed bed should be as homogeneous as possible over the cross-section, but at the same time, the temperature change at the beginning of the charging or discharging should be as steep as possible.

Further investigations are necessary to quantify the influences of the inlet temperature on the packed bed. Moreover, additional studies should be carried out to validate the numerical data with the experimental data for liquid metal energy storage. The behavior of the inlet temperature in the packed bed was not only observed for the charging but equivalently for the discharging process.

Since the charging and discharging process behaved comparably, only the charging process is discussed in the following.

4.4. Variation of the LBE mass flow

Fig. 11 shows the dependence of the vertical temperature profile on the mass flow for different relative charging times. The mass flow was varied from 1.23 kg/min to 6.82 kg/min. The difference in temperature between the energy storage at the beginning of the experiment and the entering fluid was, as in Fig. 7, approximately 200 K. The inlet temperature is given in more detail in Tab. 5, the maximum temperature difference along the vertical axis was about 0.7 K for $T_{\min,\text{set}}$.

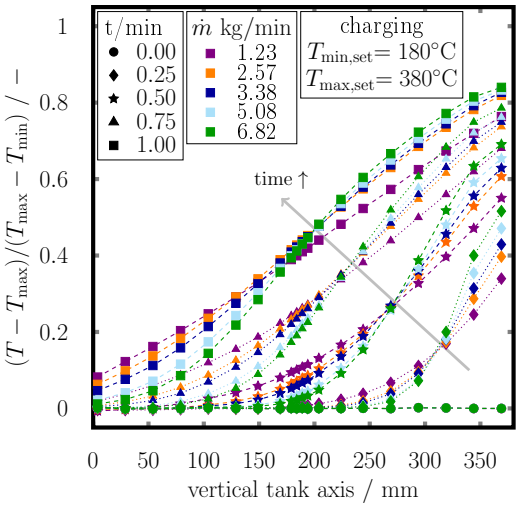

Figure 11: Temperature along the vertical axis of the energy storage tank filled with zirconium silicate spheres at same relative charging time (beginning, 25%, 50%, 75% and end of charging process).

It was observed that higher incoming mass flow rates correlated with steeper temperature profiles along the vertical axis of the energy storage container.

This could be due to the higher flow velocity and thus an increased heat transfer coefficient. Therefore, the higher the incoming mass flow, the faster the particles would be heated, making a steeper thermocline and higher maximum temperature at the energy storage inlet achievable.

The heat transfer coefficient is dependent on the flow regime present in the tank. However, the categorization of the flow regime with the mass flow based on the literature is difficult due to different Reynolds (Re) number definitions [24, 25] and varying critical Re number given for the transition of the flow regimes [26]. Nevertheless, all literature reviewed [26, 25, 27, 28, 29, 30] has in common that the Re numbers in the VESPA experiment were lower than the critical Re number for the fully turbulent flow.

The consideration of the Re number can only give an orientation regarding the flow range the experiments were carried out, on the one hand because of the large deviations of the critical Re numbers for different flow regimes and on the other hand because these experiments were all carried out with liquid metal and ceramic spheres, which in turn could affect the critical Re number. The surface texture of

the spheres may significantly influence the critical Reynolds number [26].

In addition to the difficulty of determining the flow regime, to the best of the authors' knowledge, there is no correlation for heat transfer coefficients of fluids with low Prandtl numbers flowing through fixed beds. The effect on an improved heat transfer coefficient due to a higher mass flow can not be quantitatively be proofed. Melissari and Argyropoulos [31] proposed a correlation for the determination of a heat transfer coefficient, which is also valid for low Prandtl number fluids, but only for a single sphere. Further research is needed to determine the impact of improved heat transfer due to a higher flow velocity.

Moreover, it must be kept in mind that, at the lowest mass flow rate examined here, the charging process when the inlet temperature was quite constant took 62.8 min and at the highest mass flow it took only 9.6 min, as can be seen in Tab. 5.

Table 5: Charging time and inlet temperature depending on mass flow

$\dot{m}$ kg/min	t_{const} min	t_{const}/t_{total}	T_{target} °C	T_{in} °C
1.23	62.8	95.7	380.2 ± 0.2	377.6 ± 2.3
2.57	29.7	95.6	383.2 ± 0.2	380.8 ± 2.2
3.38	21.7	96.6	384.6 ± 0.1	382.4 ± 2.0
5.08	13.5	95.9	385.4 ± 0.1	383.1 ± 2.3
6.82	9.6	96.0	386.1 ± 0.3	384.2 ± 1.6

Due to the significantly longer charging time at low mass flows, there is significantly more time for temperature equalization processes. Only at the largest mass flow is the temperature at the lowest point of the thermocouple lance still at the initial temperature. The lower the mass flow becomes, the more the temperature rises at the bottom of the energy storage. Further investigations are needed to evaluate if the effect of shorter charging time is reduced heat conductivity, or if the improved heat transfer due to higher flow velocity is dominating. Since the mass flows in this system could only be investigated in a relatively small range, the question of whether larger mass flows above a certain velocity could also have a negative effect on the temperature stratification due to flow turbulence must be investigated in the future using the DUO-LIM storage system.

4.5. Comparison of the energy storage with and without filler

Fig. 12 shows the temperature profiles along the vertical axis for different fixed bed porosities. In the experiments, the initial temperature in the energy storage was about 180 °C, and the mass flow of about 5 kg/min was also comparable for both experiments within the standard deviations. The inlet temperature of the experiment with filler was about 383.11 ± 2.3 °C, whereas the inlet temperature of the experiment without filler was on average about 381.8 ± 2.4 °C. Therefore, the experiments are comparable regarding their inlet temperature. The light blue symbols represent the temperatures for an energy storage filled with LBE only, for times from 0 to 9 min. The dark blue symbols show the temperatures for the energy storage filled with zirconium silicate spheres, (diameter 2.5–2.8 mm) with a packed bed porosity of 0.37, for the same charging times as for the energy storage filled with LBE only. It can be observed that the temperature profiles of the energy storage with a packed bed are significantly steeper than when only LBE is in the energy storage. This shows that better temperature stratification can be achieved by adding spheres with a lower thermal heat conductivity than LBE.

In both experiments, the charging process was stopped as soon as the characteristic temperature in the center of the energy storage was reached. Due to the better temperature stratification in the test with filler material, the characteristic temperature is reached after 14 min and not after 9 min. The gray symbols in Fig. 12 represent the additional temperature profiles until the characteristic temperature is reached in the center of the energy storage for the case of a packed bed in the energy storage. It can be concluded that under these experimental parameters, more energy can be stored in the energy storage with zirconium silicate as filler than in an energy storage with LBE only.

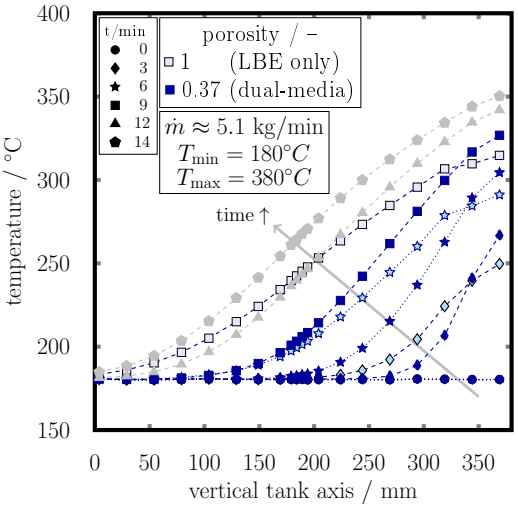

Figure 12: Temperature profiles along the vertical axis of the energy storage tank for different points in time for a charging process with T_{min}=180 °C and T_{max}=380 °C applied. The light blue data points show the results for LBE only in the the energy storage and the dark blue and the light gray data points show the results using zirconium silicate as filler.

4.6. Standby experiments

As already mentioned above in section 3.1, following every (dis)charging process, a standby experiment is carried out. Fig. 13 shows the results of the standby experiment

after the charging of the energy storage at an initial temperature of 180.3 °C with a mass flow of 6.82 kg/min at 384.2 °C, which was presented in section 4.4.

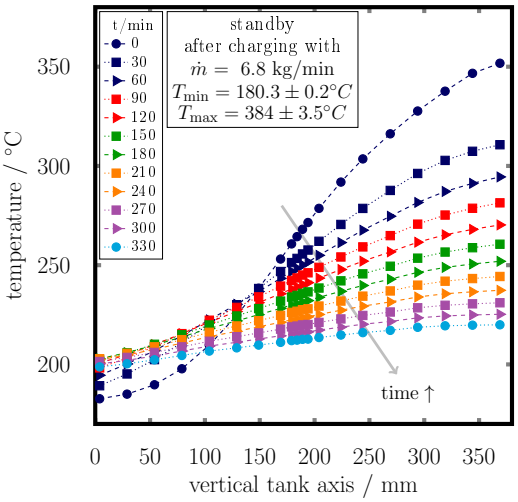

Figure 13: Temperature profiles along the vertical tank axis for the standby experiment every 30 min after the charging of the energy storage at an applied initial temperature of 180 °C with a mass flow of 6.82 kg/min at about 380 °C.

The vertical temperature profile is shown every 30 min from the start of the standby phase until a minimal temperature difference between top and bottom of 20 K was reached. It was observed that within the first 30 min the temperature at the top of the energy storage decreases the most (about 40 K), compared with the following 30 min. At the same time, at the bottom of the energy storage, the temperature increased only about 6.5 K. As time progresses, the temperature profiles flatten. After some time, the slope of the curve does not change significantly anymore, but the temperatures at each measuring point decreased.

Fig. 14 shows the vertical temperature profiles for the first hour of the standby phase in more detail by time steps of 5 min.

During the standby experiment, several processes run in parallel. Heat was lost to the environment causing cooling of the energy storage, and at the same time, heat conduction occurred within the energy storage, causing a growth of the thermocline and the temperatures at the top and the bottom of the energy storage equalized. Heat losses are significant, especially in such small thermal storage systems on a laboratory scale, since they have an unfavorable surface-to-volume ratio. In addition, high temperatures within the energy storage lead to a high temperature gradient to the environment resulting in larger heat losses through the tank wall. For this reason, good thermal insulation is necessary, especially for thermal storage systems of this type.

Heat conduction within the energy storage device is proportional to the temperature gradient. Therefore, it is to be expected that the largest temperature loss occurs at the top of the energy storage right at the beginning of the

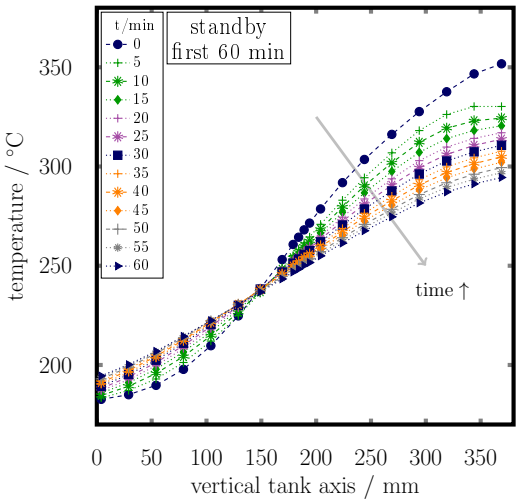

Figure 14: Temperature profiles along the vertical tank axis for the standby experiment are shown in Fig. 13. Here, the temperature profiles for the first 60 min of the experiments are shown for every 5 min.

standby process. It is noticeable that the fluid temperature at the top (where the hot fluid entered during charging process) dropped significantly more than it rose at the bottom.

In addition to the effects just mentioned, the heat capacity of the flange on the top of the energy store could influence the fluid temperature significantly. The potential influence of the flange is discussed in 4.2 in detail. It is possible that the flange at the end of the charging process is not at the same temperature as the incoming fluid. Due to the resulting temperature gradient between the hot fluid and the colder flange, the fluid at the top of the flange would cool down faster. However, a detailed knowledge of the flange temperature is required to quantify the influence, which was not available in the VESPA experiment. Furthermore, the core temperature of the particles could not yet be at equilibrium. This would lead to a further heat sink within the reservoir, which influences the temperature more at the beginning of the standby process.

5. Lessons learned

The working principle of a dual-media thermocline energy storage with liquid metal was demonstrated and lessons learned from the small-scale VESPA experiment will be applicable for the scale-up of the storage device in DUO-LIM, even if the VESPA energy storage had an unfavorable volume to surface ratio.

The concept of measuring the fluid temperature by thermocouples fixed in a lance is a suitable method for a measurement at a well-defined position along the vertical axis of the energy storage. All thermocouples are still operating after a year of experimentation, including several charging and discharging cycles.

The homogeneity of the packed bed porosity was influenced by the bounding wall of the storage tank. The inhomogeneity in porosity can influence the flow pattern and the heat transfer, but can be neglected if the ratio of the tube diameter to the particle diameter is smaller than 20 [32]. In the VESPA experiment, this ratio was between 46 and 52 for a sphere diameter of 2.5 mm to 2.8 mm, and thus, boundary effects along the wall on the packed bed may be neglected. With an appropriate choice of the sphere diameter for the packed bed filler for DUO-LIM, no other influences from the packed bed are expected.

Furthermore, no changes in (dis)charging behavior during the measurement campaign could be determined, which would refer to changes in the filler material encountered during or after cycling. Further investigation needs to be carried out to determine the long term cyclability.

The design of the region between where the fluid enters the energy storage and the packed bed should be the focus of further investigation, since the temperature entering the packed bed should change in one step to the (dis)charging temperature. When optimizing the inlet area of the energy storage, on the one hand a uniformity of the flow velocity over the entire cross-section of the packed bed should be achieved as far as possible, but at the same time, a temperature step of the fluid entering the packed bed should be realized to improve the vertical temperature profile. The diameter of the supply pipes to the thermal energy storage directly influence the heat losses of the thermal energy storage during standby due to the high heat conductivity of liquid metals. Heat losses via the supply pipes certainly have a greater impact on small energy storage systems than on large storage systems.

Future construction of the energy storage should be optimized with special focus on the heat capacity of the structural material. In particular, for small thermal energy storage systems, the heat capacity of the structural material influences the performance of the energy storage itself. The construction of the thermal energy storage system would optimally be as light as possible, as well as constructed using a material with a low heat capacity.

6. Conclusion

The first laboratory experiment on a sensible dual-media thermocline storage system with liquid lead-bismuth eutectic (LBE) as the heat transfer fluid and zirconium silicate spheres as packed bed filler material was successful. In this paper, the setup, as well as first results of the experimental facility called VESPA, are presented. The VESPA experiment provides information about important influencing parameters and design requirements for the larger scale storage system called DUO-LIM, which is to be realized in due course and will have 100 times the capacity. The results of the VESPA energy storage presented here focuses on the parameters influencing the temperature profile along the vertical tank axis of the energy storage. While some quantitative data suffer from the unfavorable volume-to-surface ratio or the large heat capacity of the flanges, which are specific to the experimental VESPA facility, many valuable results are achieved:

- The energy storage behaves similarly during charging and discharging cycles for a medium mass flow and same temperature difference.
- Higher mass flow rates steepen the temperature profile along the vertical axis of the energy storage. Improved heat transfer coefficients as well as shorter charging times, might be responsible for the observed improvement. Due to the lack of Nusselt number correlations for low Prandtl number fluids in packed beds, the influence can not be determined. It must be noted that the mass flows were varied in a small range due to facility limitations. Further investigations in the DUO-LIM energy storage need to be carried out to verify the measurements.
- The inlet temperature of the packed bed has a strong influence on the stratification in the energy storage system. Numerical investigations show that an ideal temperature step of the fluid entering the packed bed leads to a steeper thermocline profile, separating the hot and cold zones in the energy storage. The inlet temperature of the packed bed in the VESPA experiment, on the other hand, can be described by an exponential function that never reached the maximum inlet temperature to the storage tank. This resulted in a flatter thermocline profile in the simulations, where the thermocline is extended over the entire energy storage. This should be taken into account when designing future mixing inlet zones before the packed bed.
- The (dis)charging behavior can be improved by using a solid filler with a lower heat conductivity than that of the heat transfer fluid, over an energy storage filled with LBE only. Nevertheless, the thermocline extends over the entire tank height in the VESPA energy storage. Therefore, further investigations about the filler material and an improvement of the packing density of the packed bed are necessary.
- The temperature measured at the top of the vertical lance reaches only about 80% of the inlet temperature measured at the inlet of the energy storage for charging. This is equivalent for discharging. Possible reasons for the lower packed bed inlet temperature when compared to the inlet temperature of the energy storage tank are discussed. For a more precise localization and the influence of heat losses, as well as the influence on the mixing of the flows and inhomogeneities in the area between the packed bed and the flange, further temperature measurements or simulations are necessary.
- The mass flow determination of the VESPA facility using the differential pressure sensor works, but is

not ideal, particularly for small flows. However, in the planned DUO-LIM pilot scale facility, the mass flow will be determined using a Coriolis mass flow meter, which provides more accurate values.

- The energy storage of the VESPA experiment has a storage capacity of approximately 1 kWh. Thus, the influence of heat losses is huge compared to a larger thermal energy storage. Furthermore, the design of the energy storage is not ideal because of the huge heat capacity of the flanges at the top and the bottom of the energy storage. These influences can be seen during (dis)charging as well as during standby experiments. Therefore, the energy storage tank needs to be optimized to either reduce storage tank mass or alter materials for the pilot scale experiment DUO-LIM.
- This work focuses on the demonstration and design aspects of a dual-media energy storage. Further research for an optimized low-cost filler material is necessary to make the thermal energy storage more cost-effective.

Acknowledgment

The authors thank the students who worked on the VESPA experiment, especially K. Dieterle, M. Gothe and U. Koller. Furthermore, we would like to acknowledge K. Wittemann for his work in setting up the plant and E. Kleinert (Saint Gobain), who kindly provided us with the material data of the filler material of the dual-media energy storage.

Nomenclature

Acronyms

DUO-LIM	Dual-media thermocline heat storage with liquid metal
CAD	Computer-aided design
EDX	Energy dispersive X-ray spectroscopy
HTF	Heat transfer fluid
LBE	Lead-bismuth eutectic
SEM	Scanning electron microscope
VESPA	Preliminary test for energy storage setup

Subscripts

char	Characteristic
const	Constant
ES	Energy storage
exp	Experimental
f	Fluid
in	Inlet
max	Maximum
melt	Melting
min	Minimum
target	Target
set	Applied parameter
sim	Simulation
total	Total
VL	Vertical lance

Latin letters

c_p	Specific heat capacity /J kg^{-1} K^{-1}
d_p	Filler particle diameter / mm
D	Tank diameter / mm
H	Tank height / mm
l	Length / m
m	Mass / kg
$\dot{m}$	Mass flow / kg min^{-1}
Δp	Pressure difference / Pa
r	Radius of tank / mm
t	Time / s
T	Temperature / K or °C
v	Velocity / ms^{-1}
v_Ψ	Pore velocity in packed bed / ms^{-1}
v_0	Superficial velocity / ms^{-1}
V	Volume / m^3
x	Coordinate along tank height / -
y	Coordinate along energy storage radius / -

Greek letters

α	Heat transfer coefficient / W m^{-2} K^{-1}
Θ	Non-dimensional temperature / -
λ	Thermal conductivity / W m^{-1} K^{-1}
μ	Dynamic viscosity / Pas
ρ	Density / kg m^{-3}
τ	Non-dimensional time / -
Ψ	Porosity / -

Non-dimensional parameters

Re	Reynolds number

References

[1] T. Fleiter, R. Elsland, M. Rehfeldt, U. R. Jan Steinbach, G. Catenazzi, M. Jakob, C. Rutten, R. Harmsen, F. Dittmann, P. Rivière, P. Stabat, Profile of heating and cooling demand in 2015, Technical Report D3.1, Heat Roadmap Europe, 2017.

[2] G. Alva, Y. Lin, G. Fang, An overview of thermal energy storage systems, Energy 144 (2018) 341–378.

[3] K. Niedermeier, Numerical investigation of a thermal storage system using sodium as heat transfer fluid (PhD thesis, KIT Scientific Reports; KIT-SR 7755) (2019).

[4] G. Bianchi, G. P. Panayiotou, L. Aresti, S. A. Kalogirou, G. A. Florides, K. Tsamos, S. A. Tassou, P. Christodoulides, Estimating the waste heat recovery in the european union industry, Energy, Ecology and Environment 4 (2019) 211–221.

[5] N. Boerema, G. Morrison, R. Taylor, G. Rosengarten, Liquid sodium versus Hitec as a heat transfer fluid in solar thermal central receiver systems, Solar Energy 86 (2012) 2293 – 2305.

[6] J. Coventry, C. Andraka, J. Pye, M. Blanco, J. Fisher, A review of sodium receiver technologies for central receiver solar power plants, Solar Energy 122 (2015) 749–762.

[7] A. Heinzel, W. Hering, J. Konys, L. Marocco, K. Litfin,

G. Mueller, J. Pacio, C. Schroer, R. Stieglitz, L. Stoppel, A. Weisenburger, T. Wetzel, Liquid metals as efficient high temperature heat transport fluids, Energy Technology 5 (2017).
[8] J. Pacio, C. Singer, T. Wetzel, R. Uhlig, Thermodynamic evaluation of liquid metals as heat transfer fluids in concentrated solar power plants, Applied Thermal Engineering 60 (2013) 295 – 302.
[9] D. Frazer, E. Stergar, C. Cionea, P. Hosemann, Liquid metal as a heat transport fluid for thermal solar power applications, Energy Procedia 49 (2014) 627–636.
[10] J. Pacio, M. Daubner, F. Fellmoser, K. Litfin, T. Wetzel, Experimental study of heavy-liquid metal (lbe) flow and heat transfer along a hexagonal 19-rod bundle with wire spacers, Nuclear Engineering and Design 301 (2016) 111–127.
[11] A. Alemberti, V. Smirnov, C. F. Smith, M. Takahashi, Overview of lead-cooled fast reactor activities, Progress in Nuclear Energy 77 (2014) 300–307.
[12] J.-S. Kim, A. Dawson, R. Wilson, K. Venkatesan, W. Stein, High-Temperature Heat Transport and Storage Using LBE Alloy for Concentrated Solar Power System (2015).
[13] Thermal energy storage technologies for concentrated solar power – a review from a materials perspective, Renewable Energy 156 (2020) 1244–1265.
[14] B. D. Pomeroy, Thermal energy storage in a packed bed of iron spheres with liquid sodium coolant, Solar Energy 23 (1979) 513–515.
[15] OECD-NEA, Handbook on Lead-bismuth Eutectic Alloy and Lead Properties, Materials Compatibility, Thermal-hydraulics and Technologies, OECD/NEA Nuclear Science Committee Working Party on Scientific Issues of the Fuel Cycle Working Group on Lead-bismuth Eutectic, 2015.
[16] R. G. Ballinger, J. Lim, An overview of corrosion issues for the design and operation of high-temperature lead- and lead-bismuth-cooled reactor systems, Nuclear Technology 147 (2004) 418–435.
[17] J. Zhang, N. Li, Review of the studies on fundamental issues in LBE corrosion, Journal of Nuclear Materials 373 (2008) 351–377.
[18] M. Popovic, A. Bolind, Y. Aussat, A. Gubser, P. Hosemann, Oxidative passivation of fe–cr–al steels in lead-bismuth eutectic under oxygen-controlled static conditions at 700 °C and 800 °C, Journal of Nuclear Materials 523 (2019) 172–181.
[19] J.-B. Vogt, I. PRORIOL Serre, A review of the surface modifications for corrosion mitigation of steels in lead and lbe, Coatings 11 (2021) 53.
[20] G. Angelini, A. Lucchini, G. Manzolini, Comparison of thermocline molten salt storage performances to commercial two-tank configuration, Energy Procedia 49 (2014) 694–704.
[21] J. E. Pacheco, S. K. Showalter, W. J. Kolb, Development of a molten-salt thermocline thermal storage system for parabolic trough plants, Journal of Solar Energy Engineering 124 (2002) 153–159.
[22] E. Kleinert, private communication, 2020. Material data Rimax (Saint Gobain).
[23] K. Niedermeier, L. Marocco, J. Flesch, G. Mohan, J. Coventry, T. Wetzel, Performance of molten sodium vs. molten salts in a packed bed thermal energy storage, Applied Thermal Engineering 141 (2018) 368–377.
[24] A. Della Torre, G. Montenegro, G. Tabor, M. Wears, Cfd characterization of flow regimes inside open cell foam substrates, International Journal of Heat and Fluid Flow 50 (2014) 72–82.
[25] D. Seguin, A. Montillet, J. Comiti, Experimental characterisation of flow regimes in various porous media–I: Limit of laminar flow regime, Chemical Engineering Science 53 (1998) 3751–3761.
[26] Özer Bağcı, N. Dukhan, M. Özdemir, Flow regimes in packed beds of spheres from pre-darcy to turbulent, Transport in Porous Media 104 (2014) 501–520.
[27] R. M. Fand, B. Y. K. Kim, A. C. C. Lam, R. T. Phan, Resistance to the Flow of Fluids Through Simple and Complex Porous Media Whose Matrices Are Composed of Randomly Packed Spheres, Journal of Fluids Engineering 109 (1987) 268–273.
[28] K. Jolls, T. Hanratty, Transition to turbulence for flow through a dumped bed of spheres, Chemical Engineering Science 21 (1966) 1185–1190.
[29] D. Seguin, A. Montillet, J. Comiti, F. Huet, Experimental characterization of flow regimes in various porous media–II: Transition to turbulent regime, Chemical Engineering Science 53 (1998) 3897–3909.
[30] T. H. Wegner, A. J. Karabelas, T. J. Hanratty, Visual studies of flow in a regular array of spheres, Chemical Engineering Science 26 (1971) 59–63.
[31] B. Melissari, S. A. Argyropoulos, Development of a heat transfer dimensionless correlation for spheres immersed in a wide range of prandtl number fluids, International Journal of Heat and Mass Transfer 48 (2005) 4333–4341.
[32] M. Stieß, Mechanische Verfahrenstechnik - Partikeltechnologie 1, 3 ed., Springer Berlin Heidelberg, 2009.